

UC San Diego

UC San Diego Previously Published Works

Title

Genetic dissection of the Down syndrome critical region

Permalink

<https://escholarship.org/uc/item/3xj3t0qb>

Journal

Human Molecular Genetics, 24(22)

ISSN

0964-6906

Authors

Jiang, Xiaoling
Liu, Chunhong
Yu, Tao
et al.

Publication Date

2015-11-15

DOI

10.1093/hmg/ddv364

Peer reviewed

ORIGINAL ARTICLE

Genetic dissection of the Down syndrome critical region

Xiaoling Jiang^{1,†}, Chunhong Liu^{1,†}, Tao Yu^{1,2,†}, Li Zhang^{1,3,†}, Kai Meng^{1,3}, Zhuo Xing¹, Pavel V. Belichenko⁴, Alexander M. Kleschevnikov⁴, Annie Pao¹, Jennifer Peresie¹, Sarah Wie¹, William C. Mobley^{4,‡} and Y. Eugene Yu^{1,5,‡,*}

¹The Children's Guild Foundation Down Syndrome Research Program, Genetics Program and Department of Cancer Genetics, Roswell Park Cancer Institute, Buffalo, NY 14263, USA, ²Department of Medical Genetics, Tongji Medical College, Huazhong University of Science and Technology, Wuhan, Hubei 430030, China, ³Department of Physiology and Pathophysiology, Medical School of Xi'an Jiaotong University, Xi'an, Shaanxi 710061, China, ⁴Department of Neurosciences, School of Medicine, University of California at San Diego, La Jolla, CA 92093, USA and ⁵Genetics, Genomics and Bioinformatics Program, Department of Cellular and Molecular Biology, Roswell Park Division of Graduate School, State University of New York at Buffalo, Buffalo, NY 14263, USA

*To whom correspondence should be addressed. Tel: +1 7168451099; Fax: +1 7168451698; Email: yuejin.yu@roswellpark.org

Abstract

Down syndrome (DS), caused by trisomy 21, is the most common chromosomal disorder associated with developmental cognitive deficits. Despite intensive efforts, the genetic mechanisms underlying developmental cognitive deficits remain poorly understood, and no treatment has been proven effective. The previous mouse-based experiments suggest that the so-called Down syndrome critical region of human chromosome 21 is an important region for this phenotype, which is demarcated by *Setd4/Cbr1* and *Fam3b/Mx2*. We first confirmed the importance of the *Cbr1-Fam3b* region using compound mutant mice, which carry a duplication spanning the entire human chromosome 21 orthologous region on mouse chromosome 16 [*Dp(16)1Yey*] and *Ms1Rhr*. By dividing the *Setd4-Mx2* region into complementary *Setd4-Kcnj6* and *Kcnj15-Mx2* intervals, we started an unbiased dissection through generating and analyzing *Dp(16)1Yey/Df(16Setd4-Kcnj6)Yey* and *Dp(16)1Yey/Df(16Kcnj15-Mx2)Yey* mice. Surprisingly, the *Dp(16)1Yey*-associated cognitive phenotypes were not rescued by either deletion in the compound mutants, suggesting the possible presence of at least one causative gene in each of the two regions. The partial rescue by a *Dyrk1a* mutation in a compound mutant carrying *Dp(16)1Yey* and the *Dyrk1a* mutation confirmed the causative role of *Dyrk1a*, whereas the absence of a similar rescue by *Df(16Dyrk1a-Kcnj6)Yey* in *Dp(16)1Yey/Df(16Dyrk1a-Kcnj6)Yey* mice demonstrated the importance of *Kcnj6*. Our results revealed the high levels of complexities of gene actions and interactions associated with the *Setd4/Cbr1-Fam3b/Mx2* region as well as their relationship with developmental cognitive deficits in DS.

Introduction

Human trisomy 21 [Down syndrome (DS)] is the most common chromosomal abnormality associated with developmental cognitive deficits in the human population (1,2), occurring in one in approximately 691 and 1000 newborns in the USA (3) and Europe (4), respectively. In addition, the pregnancy termination rate

after pre-natal diagnosis of human trisomy 21 has not increased, and the incidence rate of DS has not decreased in the last decade in countries such as the USA, due partly to improved medical care and social support for individuals with DS (5). However, despite improved medical care, there is still no effective treatment available to improve cognitive function for individuals with DS. Therefore, there is a particularly urgent need to explore in depth the

[†]The authors wish it to be known that, in their opinion, the first four authors should be regarded as joint First Authors.

[‡]W.C.M. and Y.E.Y. contributed equally to this paper.

Received: June 12, 2015. Revised: August 10, 2015. Accepted: September 2, 2015

© The Author 2015. Published by Oxford University Press. All rights reserved. For Permissions, please email: journals.permissions@oup.com

genetic mechanisms underlying developmental cognitive deficits in DS to facilitate the development of new interventions.

To establish genotype–phenotype relationships, several groups have examined human segmental trisomies. In these studies, data generated from patients with segmental trisomy of human chromosome 21 (Hsa21) were used to map genomic regions associated with DS phenotypes. During these investigative efforts, the Down syndrome critical region (DSCR) was defined and proposed to be responsible for major DS phenotypes, including developmental cognitive deficits (6,7). Unfortunately, interpretation of the genotype–phenotype relationships inferred from these studies is complicated because some patients with segmental trisomy 21 carried additional chromosomal anomalies. For instance, through translocation, some individuals were segmentally trisomic for other chromosomes (6,7). Another problem is that the triplication endpoints almost always differ in each case of segmental trisomy, which makes it difficult to distinguish the contributions of trisomy from individual difference (8).

To pursue an alternative strategy for establishing the genotype–phenotype relationship, mouse models have been generated on the basis of evolutionary conservation between Hsa21 and three regions of the mouse genome located on mouse chromosome 10 (Mmu10), Mmu16 and Mmu17. The Hsa21 orthologous region on Mmu16 is the largest one and contains ~65.7% of all the Hsa21 gene orthologs (Fig. 1). Triplication of this region caused developmental cognitive deficits in *Dp(16)1Yey/+*, abbreviated as *Dp(16)1/+*, mice (9). The mouse DSCR, demarcated by *Setd4/Cbr1* and *Fam3b/Mx2*, is located within this region (Fig. 1 and Supplementary Material, Table S1). Mouse-based experimental results support the proposal that the *Setd4/Cbr1-Fam3b/Mx2* region plays a critical role in causing developmental cognitive

deficits (10–12). Of 29–31 Hsa21 gene orthologs in the region, *Dyrk1a* and *Kcnj6* are considered important candidates for contributing to this phenotype (10). It is possible that these and other genes in the *Setd4/Cbr1-Fam3b/Mx2* region contribute to the phenotypes by interacting directly and/or indirectly among themselves and/or with other triplicated genes. In this study, we set out to examine these possibilities by generating and analyzing mouse mutants carrying specific genetic alterations.

Results

Confirmation of the impact of the *Cbr1-Fam3b* region using *Dp(16)1;Ms1Rhr* mice

The mouse DSCR is located in the Hsa21 orthologous region on Mmu16, which is demarcated by *Setd4/Cbr1* and *Fam3b/Mx2* (Fig. 1 and Supplementary Material, Table S1). *Dp(16)1*, a duplication spanning the entire Hsa21 orthologous region on Mmu16, serves as a reference for genetic dissection of the *Setd4/Cbr1-Fam3b/Mx2* region (Fig. 1) (13). The presence of *Dp(16)1/+* caused impairment of cognitively relevant phenotypes in mice, including contextual fear conditioning and hippocampal long-term potentiation (LTP) (9) which is viewed as a major physiological phenomenon associated with learning and memory (14,15). We have previously shown that reducing the copy number of the *Cbr1-Fam3b* region from three to two rescued impaired hippocampal LTP caused by the presence of *Dp(16)1* (12). In this study, we extended the analysis of the *Cbr1-Fam3b* region by including the T-maze spontaneous alternation test and the contextual fear-conditioning test. The T-maze test has been used to reveal functional abnormalities of the mouse hippocampal system. The contextual fear-conditioning test has been used to examine the capacity for hippocampal-mediated contextual memory in mice. Both tests have been used extensively to analyze mouse models of DS (9,10,16). In the T-maze test, *Dp(16)1/+* mice performed significantly worse than wild-type controls ($P < 0.01$). But converting the *Cbr1-Fam3b* to two copies rendered the difference of the performances between *Dp(16)1;Ms1Rhr* mice and wild-type controls insignificant ($P = 0.247$), even though the difference between *Dp(16)1;Ms1Rhr* and *Dp(16)1/+* mice is not significant either ($P = 0.085$; Fig. 2A). In the contextual fear-conditioning test, mice of all genotypes had a similar low baseline freezing level before presentation of the foot shock ($P > 0.05$; Fig. 2B). *Dp(16)1;Ms1Rhr*, *Dp(16)1/+* and $+/+$ mice showed elevated

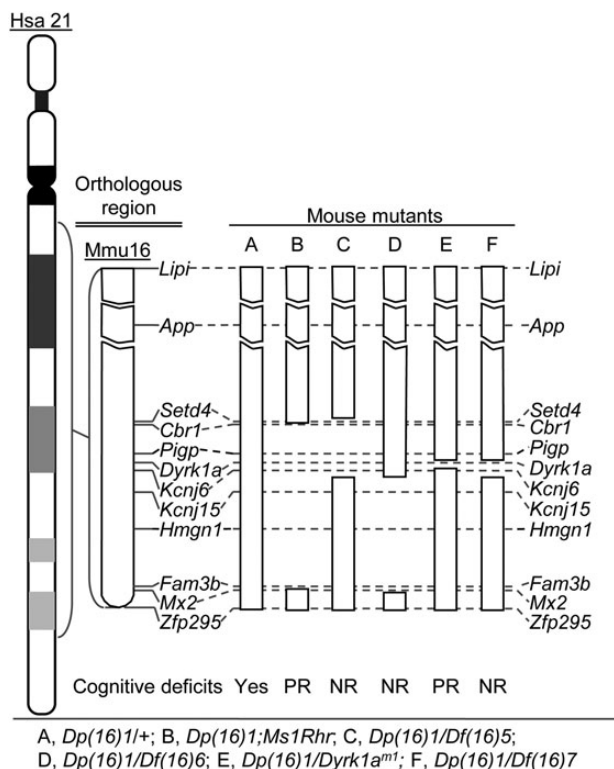


Figure 1. Mouse mutants and their cognitive phenotypes. Hsa21 and the orthologous region on Mmu16 are shown. Dashed lines indicate the locations of specific genes. PR, partial rescue observed; NR, no rescue observed.

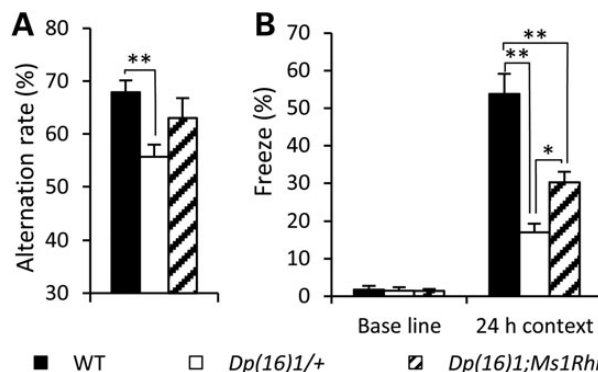


Figure 2. Analysis of *Dp(16)1;Ms1Rhr* mice. (A) *Dp(16)1;Ms1Rhr* ($n = 15$), *Dp(16)1/+* ($n = 13$) and $+/+$ ($n = 13$) mice were examined in the T-maze. (B) The three groups of mice in (A) were examined in a contextual fear-conditioning test. The percentages of time frozen before the foot shock and during the 24 h contextual tests are shown. * $P < 0.05$ and ** $P < 0.01$.

freezing behavior when they were returned to the test chamber 24 h after the initial training and foot shock. Similar to our previous observations, *Dp(16)1/+* mice froze significantly less than wild-type controls ($P < 0.01$) (Fig. 2B) (9). Additional comparative analysis showed that *Dp(16)1;Ms1Rhr* mice froze significantly more than *Dp(16)1/+* mice ($P < 0.05$), but did not reach the level achieved by wild-type controls ($P < 0.01$). To facilitate interpretation of the contextual fear condition data, we performed a foot-shock sensitivity test and detected no difference in the mean threshold of the current to elicit flinching or vocalizing between mice with the aforementioned genotypes as well as all other genotypes used in the subsequent contextual fear-conditioning tests in this study (data not shown). These results indicate that the normalization of the *Cbr1-Fam3b* region to two copies partially rescued the cognitive deficits caused by the presence of *Dp(16)1*.

Examination of the impacts of the *Setd4-Kcnj6* and *Kcnj15-Mx2* regions by generating and analyzing compound mouse mutants

After confirming the impact of the *Cbr1-Fam3b* region on cognitive behaviors using *Dp(16)1;Ms1Rhr* mice, we started the unbiased dissection of the *Setd4/Cbr1-Fam3b/Mx2* region by dividing the region into two complementary intervals. To do this, we generated *Df(16)Setd4-Kcnj6*Yey [abbreviated as *Df(16)5Yey* or *Df(16)5*] and *Df(16)Kcnj15-Mx2*Yey [abbreviated as *Df(16)6Yey* or *Df(16)6*], which have deletions of 15 and 16 Hsa21 gene orthologs, respectively (Fig. 1 and Supplementary Material, Table S1).

To generate *Df(16)5* in mouse embryonic stem (ES) cells, MICER clones MHPN267e05 and MHPP54c08 (17) were used to target loxP into the regions proximal to *Setd4* and distal to *Kcnj6*, respectively (Fig. 3A). To generate *Df(16)6* in ES cells, MICER clones MHPP54c08 and MHPN178b08 (17) were used to target loxP into the regions proximal to *Kcnj15* and distal to *Mx2*, respectively (Fig. 4A). The ES cell clones carrying *Df(16)5* and *Df(16)6* were generated by transfection of a Cre-expression vector into double-targeted ES cells and identified by Southern blot analysis (Figs 3A and 4A). The deletions were confirmed by fluorescent in situ hybridization (FISH) analysis (18,19) (Figs 3B and C and 4B and C). *Df(16)5/+* and *Df(16)6/+* mice were generated using the aforementioned ES cells and were identified by Southern blot analysis (Figs 3D and 4D). *Df(16)5/+* and *Df(16)6/+* mice appear overtly normal. Both strains showed transmission ratio distortion, with either deletion transmitted at the ratio lower than predicted.

To assess the impact on the level of mRNAs by the copy number variation of their coding genes, we analyzed expression of *App*, *Pigp*, *Dyrk1a*, *Kcnj6* and *Hmgn1* in *Dp(16)1/+*, *Dp(16)1/Df(16)5* and *Dp(16)1/Df(16)6* brains using TaqMan[®] real-time quantitative reverse transcriptase-polymerase chain reaction (RT-PCR) (Fig. 1). All five genes are present at three copies in *Dp(16)1/+* brains, but *Pigp*, *Dyrk1a* and *Kcnj6* are converted to two copies in *Dp(16)1/Df(16)5* brains and *Hmgn1* is converted to two copies in *Dp(16)1/Df(16)6* brains. The quantitative RT-PCR results showed that the detected mRNA levels reflected the copy numbers of their coding genes in the mutants (Fig. 1 and Table 1).

To analyze the impact of the *Setd4-Kcnj6* and *Kcnj15-Mx2* regions on DS-associated cognitively relevant phenotypes, we compared the phenotypes of *Dp(16)1/Df(16)5* and *Dp(16)1/Df(16)6* mice with those of *Dp(16)1/+* mice and wild-type controls. Our results showed that both *Dp(16)1/Df(16)5* and *Dp(16)1/Df(16)6* mice performed significantly worse than wild-type controls in the T-maze and contextual fear-conditioning tests ($P < 0.05$; Figs 3E and F and 4E and F). In addition, neither *Dp(16)1/Df(16)5*

nor *Dp(16)1/Df(16)6* mice showed improvement over *Dp(16)1/+* mice in these tests ($P > 0.05$; Figs 3E and F and 4E and F). To assess the impact of the *Setd4-Kcnj6* and *Kcnj15-Mx2* regions on hippocampal synaptic plasticity, we performed *in vitro* electrophysiological analysis in the CA1 region of hippocampus in brain slices with the focus on hippocampal LTP. LTP in the brain slices was induced by theta burst stimulation (TBS). Mean slopes of extracellular field excitatory post-synaptic potentials (fEPSPs) were measured for 60 min after the TBS. A comparative analysis showed that the magnitude of LTP of the synaptic response after TBS of the brain slices from *Dp(16)1/Df(16)5* and *Dp(16)1/Df(16)6* mice are significantly lower than that from wild-type controls ($P < 0.05$, Figs 3G and 4G). Further comparison showed that the magnitude of LTP after TBS of the brain slices from *Dp(16)1/Df(16)5* and *Dp(16)1/Df(16)6* mice appeared slightly higher than that from *Dp(16)1/+* mice, but the differences are not statistically significant ($P > 0.05$; Figs 3G and 4G). The behavioral and electrophysiological data indicate that converting either the *Setd4-Kcnj6* region or the *Kcnj15-Mx2* region to two copies does not rescue the cognitively relevant phenotypes caused by *Dp(16)1*. This suggests that both *Setd4-Kcnj6* and *Kcnj15-Mx2* regions contain dosage-sensitive genes and that the causative gene(s) in either region can contribute to the cognitively relevant phenotypes.

Examination of the impact of *Dyrk1a* and *Kcnj6* by generating and analyzing compound mouse mutants

We showed earlier that reducing the copy number of the *Setd4-Kcnj6* region from three to two in *Dp(16)1/Df(16)5* mice did not improve learning and memory compared with *Dp(16)1/+* mice. This result is unexpected because *Dyrk1a* and *Kcnj6*, the major candidate genes for DS-associated cognitive deficits (10), are located within this interval. *Dyrk1a* encodes a dual-specificity tyrosine-phosphorylation-regulated kinase, which plays a critical role in signaling (20–22). *Kcnj6* encodes for a G protein-activated potassium channel, which regulates neuronal excitability by mediating the inhibitory effects of G-protein-coupled receptors for neuromodulators and neurotransmitters (23,24). If copy number increases of these genes contribute to the cognitively relevant phenotypes, then normalizations of the copy number in *Dp(16)1/Df(16)5* mice should have led to improvement of cognitive function when compared with *Dp(16)1/+* mice. Therefore, we decided to examine the impact of *Dyrk1a* and *Kcnj6* using the subtractive strategy with *Dp(16)1* as the reference.

To examine the impact of *Dyrk1a*, we generated a *Dyrk1a* mutant allele in mice using the SIGTR ES cell line XQ0369, which carries *Dyrk1a*Gt(XQ0369)Wtsi (abbreviated as *Dyrk1a^{m1}*). By sequencing the RT-PCR product, we confirmed the presence of the specific fusion mRNA in the XQ0369 ES cells generated by insertion of the *beta-Geo* cassette into intron 4 of *Dyrk1a* (Fig. 5B and Supplementary Material, Fig. S1). This insertion causes a disruption in the 321-amino acid kinase domain of DYRK1A, which occurs after the first 14 amino acids encoded by exon 4. To examine the impact of *Dyrk1a* and *Kcnj6* simultaneously, we generated *Df(16)Dyrk1a-Kcnj6*Yey [abbreviated as *Df(16)7Yey* or *Df(16)7*] in mouse ES cells. MICER clones MHPN85f19 and MHPP54c08 (17) were used to target loxP into the regions proximal to *Dyrk1a* and distal to *Kcnj6*, respectively (Fig. 6A). The ES cell clones carrying *Df(16)7* were generated by transfection of a Cre-expression vector into double-targeted ES cells and identified by Southern blot analysis (Fig. 6A). The deletion was confirmed by FISH analysis (Fig. 6B and C). *Dyrk1a^{m1}/+* and *Df(16)7Yey/+* mice were generated using the aforementioned ES cells. *Dyrk1a^{m1}/+* mice were maintained using

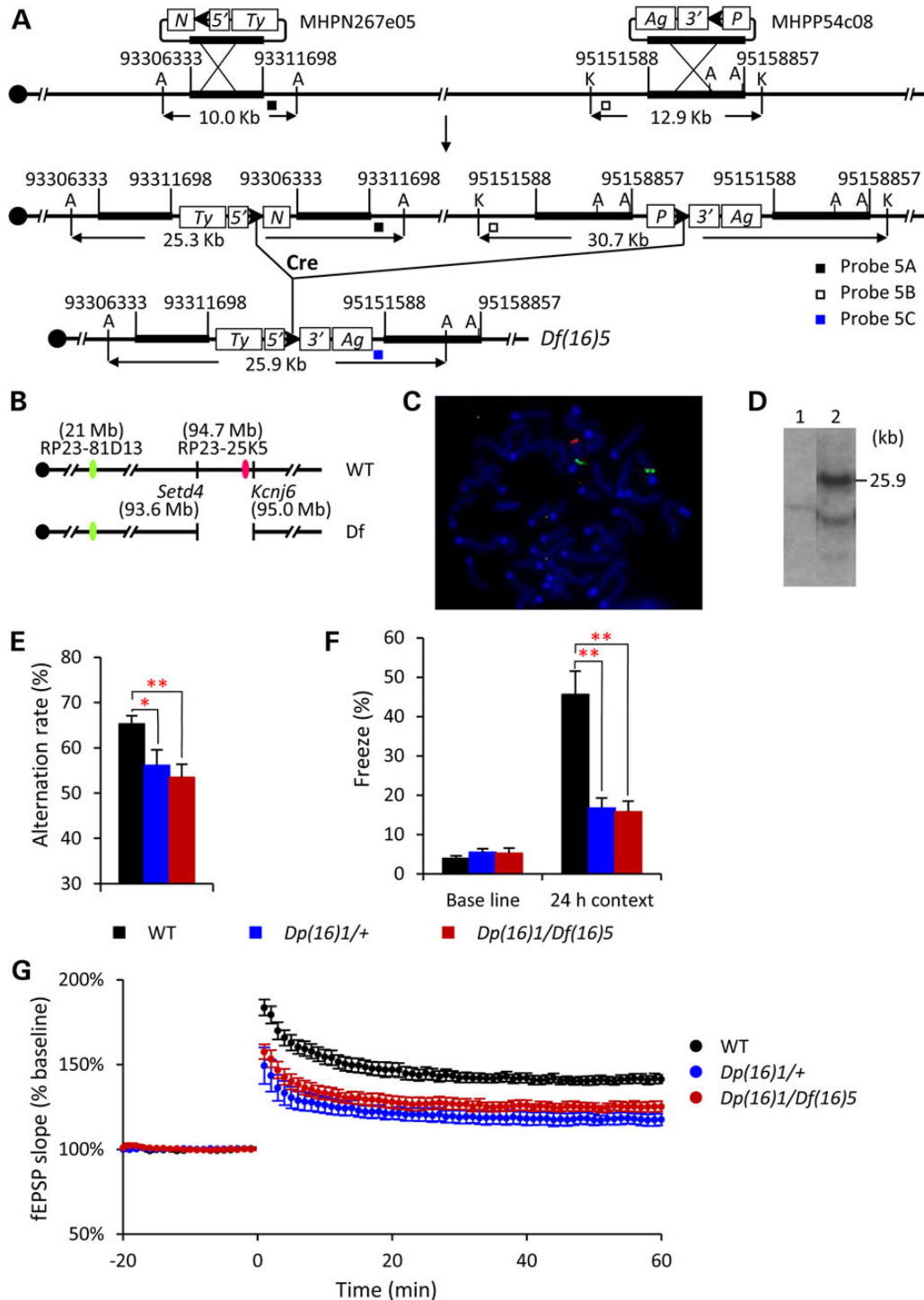


Figure 3. Generation and analysis of *Dp(16)1/Df(16)5* mice. (A) Strategy to generate *Df(16)5*. 5', 5' half of a HPRT minigene; 3', 3' half of a HPRT minigene; N, neomycin resistance gene; P, puromycin resistance gene; Ty, tyrosinase transgene; Ag, K14-Agouti transgene; \blacktriangleright , loxP; A, AflII; K, KpnI. (B) Genomic locations of BAC probes for FISH analysis. (C) FISH analysis of metaphase chromosomes prepared from *Df(16)5/+* ES cells. (D) Southern blot analysis, using Probe 5C, of AflIII-digested tail DNA from a *Df(16)5/+* mouse. (E) *Dp(16)1/Df(16)5* ($n = 13$), *Dp(16)1/+* ($n = 13$) and $+/+$ ($n = 16$) mice were examined in the T-maze. (F) The three groups of mice in (E) were examined in a contextual fear-conditioning test. The percentages of time frozen before the foot shock and during the 24 h contextual tests are shown. (G) Analysis of hippocampal LTP. Brain slices from *Dp(16)1/Df(16)5* ($n = 9$), *Dp(16)1/+* ($n = 9$) and $+/+$ ($n = 9$) mice were analyzed using electrophysiological recordings in the CA1 region of the hippocampus. Recordings of fEPSPs were carried out before and after TBS inductions. Evoked potentials were normalized to the fEPSPs recorded prior to TBS induction. * $P < 0.05$ and ** $P < 0.01$.

beta-Geo-specific PCR-based genotyping (Fig. 5A). *Dyrk1a*^{m1/+} mice appear overtly normal. After backcrossing to C57BL/6J or 129Sv mice, *Dyrk1a*^{m1/+} mice showed transmission ratio distortion with

the mutation transmitted at the ratio lower than predicted. Therefore, *Dyrk1a*^{m1/+} mice were maintained by crossing *Dyrk1a*^{m1/+} mice either with wild-type (129Sv \times C57BL/6J)F1 mice or with

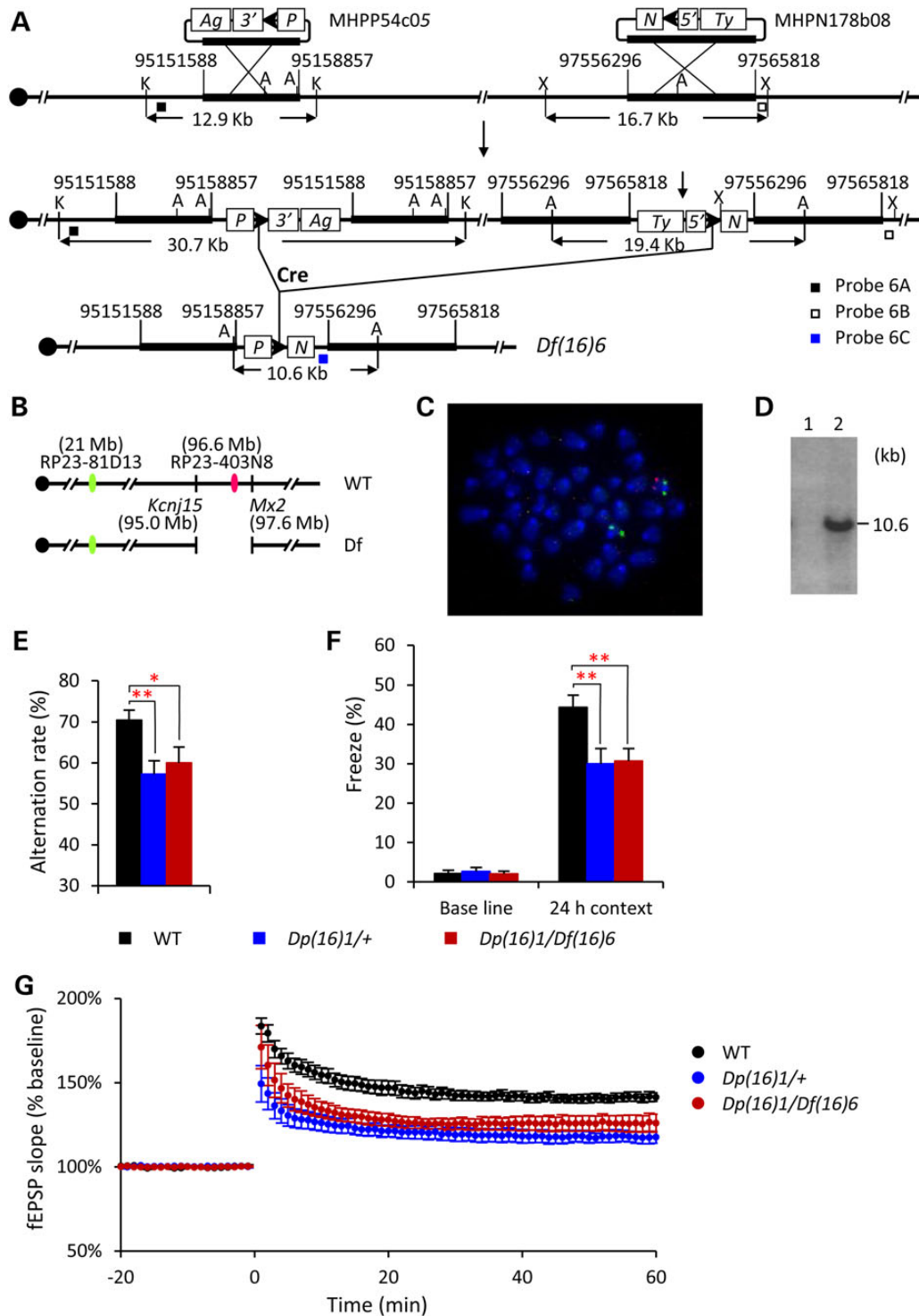


Figure 4. Generation and analysis of *Dp(16)1/Df(16)6* mice. (A) Strategy to generate *Df(16)6*. For the definitions of the abbreviations, see the legend in Figure 3A. A, AflII; K, KpnI; X, XbaI. (B) Genomic locations of BAC probes for FISH analysis. (C) FISH analysis of metaphase chromosomes prepared from *Df(16)6/+* ES cells. (D) Southern blot analysis, using Probe 6C, of AfIII-digested tail DNA from a *Df(16)6/+* mouse. (E) *Dp(16)1/Df(16)6* ($n = 10$), *Dp(16)1/+* ($n = 12$) and $+/+$ ($n = 11$) mice were examined in the T-maze. (F) The three groups of mice in (E) were examined in a contextual fear-conditioning test. The percentages of time frozen before the foot shock and during the 24 h contextual tests are shown. (G) Analysis of hippocampal LTP. Brain slices from *Dp(16)1/Df(16)6* ($n = 8$), *Dp(16)1/+* ($n = 9$) and $+/+$ ($n = 9$) mice were analyzed using electrophysiological recordings in the CA1 region of the hippocampus. Recordings of fEPSPs were carried out before and after TBS inductions. Evoked potentials were normalized to the fEPSPs recorded prior to TBS induction. * $P < 0.05$ and ** $P < 0.01$.

Dp(16)1/+ mice. Sibling mating of *Dp(16)1/Dyrk1a^{m1}* mice did not result in any viable pups carrying either the *Dp(16)1* allele or the *Dyrk1a^{m1}* allele alone, indicating that the homozygosity of either

mutation led to embryonic lethality. The embryonic lethal phenotype caused by *Dyrk1a^{m1}/Dyrk1a^{m1}* and the aforementioned mutation-associated haploinsufficiency are very similar to the

phenotypes of another *Dyrk1a* knockout mouse strain (25). *Df(16)7/+* mice were identified by Southern blot analysis (Fig. 6D). *Df(16)7Yey/+* mice appear overtly normal. The strain showed

Table 1. Normalized relative values of expression in the brains (RQ \pm SEM)*

Gene name	<i>Dp(16)1/+</i> over <i>+/+</i>	<i>Dp(16)1/Df(16)5</i> over <i>+/+</i>	<i>Dp(16)1/Df(16)6</i> over <i>+/+</i>	<i>Dp(16)1/Df(16)7</i> over <i>+/+</i>	<i>Dp(16)1/Dyrk1a^{mt1}</i> over <i>+/+</i>
<i>App</i>	1.46 \pm 0.10	1.56 \pm 0.11	1.57 \pm 0.15	1.55 \pm 0.05	1.54 \pm 0.03
<i>Pigp</i>	1.50 \pm 0.10	1.05 \pm 0.19	1.84 \pm 0.22	1.67 \pm 0.09	1.48 \pm 0.07
<i>Dyrk1a</i>	1.52 \pm 0.09	0.84 \pm 0.07	1.22 \pm 0.08	0.95 \pm 0.03	1.03 \pm 0.00
<i>Kcnj6</i>	1.37 \pm 0.06	0.87 \pm 0.09	1.23 \pm 0.08	0.96 \pm 0.06	1.28 \pm 0.05
<i>Hmgn1</i>	1.55 \pm 0.13	1.62 \pm 0.26	1.10 \pm 0.01	1.70 \pm 0.08	1.67 \pm 0.05

*The values represent the means of triplicated samples. *Gapdh* was used as an internal control and is disomic in all strains. In the Hsa21 orthologous region on Mmu16, *App* is located proximal to the *Setd4/Cbr1-Fam3b/Mx2* region, *Pigp*, *Dyrk1a* and *Kcnj6* are located within the deleted region in *Df(16)5* and *Hmgn1* is located within the deleted region of *Df(16)6*.

transmission ratio distortion with the deletion transmitted at the ratio lower than predicted.

To assess the impact on the level of mRNAs by the copy number variation of their coding genes, we analyzed expression of *App*, *Pigp*, *Dyrk1a*, *Kcnj6* and *Hmgn1* in *Dp(16)1/Dyrk1a^{mt1}* and *Dp(16)1/Df(16)7* brains using TaqMan real-time quantitative PCR. All five genes are present at three copies in *Dp(16)1Yey/+* brains, but *Dyrk1a* is converted to two copies in *Dp(16)1/Dyrk1a^{mt1}* mice and *Dyrk1a* and *Kcnj6* are converted to two copies in *Dp(16)1/Df(16)7* mice (Fig. 1). The quantitative PCR results showed that the detected mRNA levels reflected the copy numbers of their coding genes in the mutants (Fig. 1 and Table 1).

To analyze the impact of *Dyrk1a* on DS-associated cognitively relevant phenotypes, we compared *Dp(16)1/Dyrk1a^{mt1}* mice with *Dp(16)1/+* mice and wild-type controls in the T-maze and contextual fear-conditioning tests. Our results showed that *Dp(16)1/Dyrk1a^{mt1}* mice performed better than *Dp(16)1/+* mice in the T-maze and contextual fear-conditioning tests ($P < 0.01$), even though their performance did not reach the level achieved by wild-type controls ($P < 0.05$) (Fig. 5C and D). When we compared

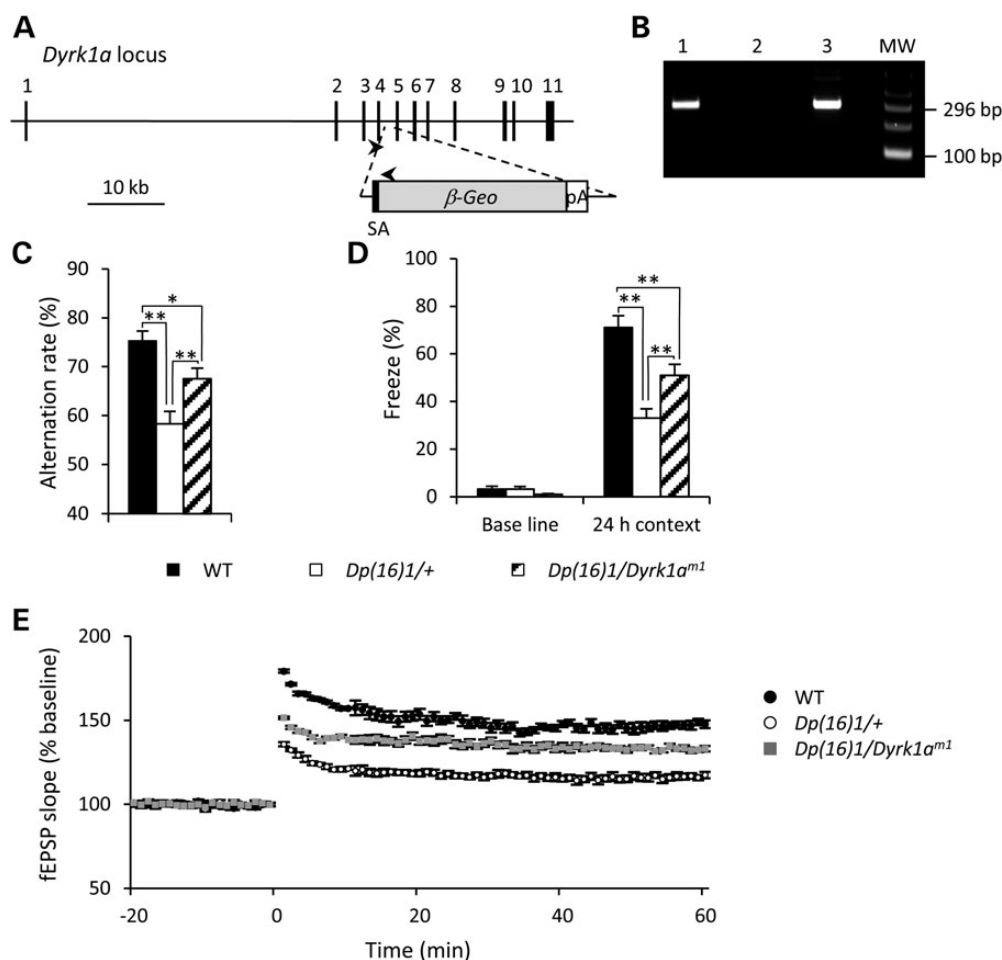


Figure 5. Generation and analysis of *Dp(16)1/Dyrk1a^{mt1}* mice. (A) The gene trap insertion site in *Dyrk1a* in the ES cell clone QX0369. Arrow heads indicate the primer locations for RT-PCR. (B) Confirmation of the gene trap event by RT-PCR. RNAs were purified from the QX0369 ES cells and the brains of a *Dyrk1a^{mt1/+}* mouse and a wild-type littermate. RT-PCR was performed using the forward primer located in exon 4 of *Dyrk1a* and the reverse primer in the *beta-Geo* cassette at the annealing temperature of 70°C. The resulting product was 296 bp. Lane 1, *Dyrk1a^{mt1/+}* mouse; lane 2, wild-type littermate; lane 3, *Dyrk1a* gene trap cell clone QX0369; MW, 100 bp DNA ladder. Sequencing of the PCR products confirms the presence of a fusion mRNA (Supplementary Material, Fig. S1). (C) *Dp(16)1/Dyrk1a^{mt1}* ($n = 16$), *Dp(16)1/+* ($n = 16$) and *+/+* ($n = 16$) mice were examined in the T-maze. (D) The three groups of mice in (C) were examined in a contextual fear-conditioning test. The percentages of time frozen before the foot shock and during the 24 h contextual tests are shown. (E) Analysis of LTP. Brain slices from *Dp(16)1/Dyrk1a^{mt1}* ($n = 13$), *Dp(16)1/+* ($n = 13$) and *+/+* ($n = 13$) mice were analyzed using electrophysiological recordings in the CA1 region of the hippocampus. Recordings of fEPSPs were carried out before and after TBS inductions. Evoked potentials were normalized to the fEPSPs recorded prior to TBS induction. * $P < 0.05$ and ** $P < 0.01$.

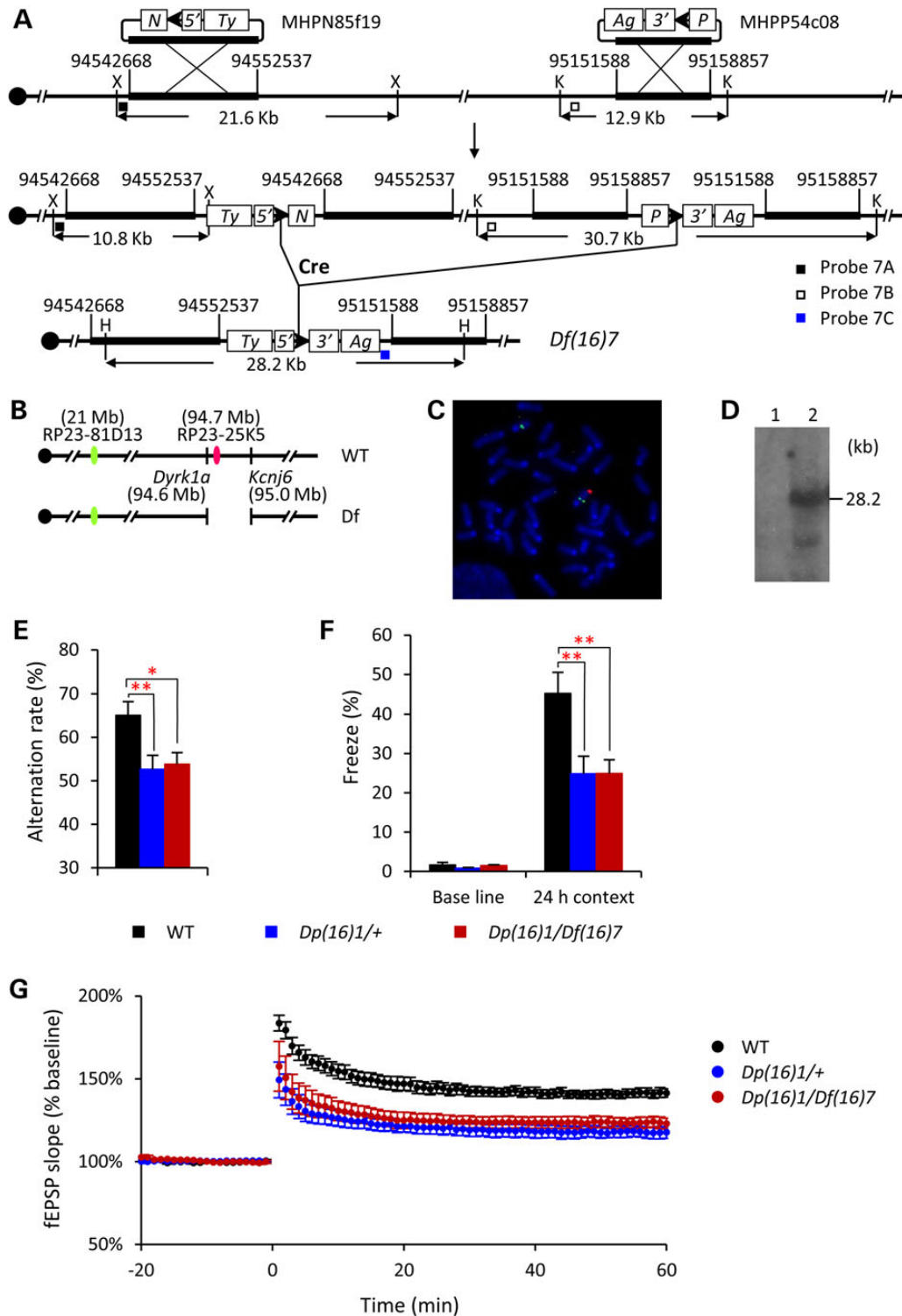


Figure 6. Generation and analysis of *Dp(16)1/Df(16)7* mice. (A) Strategy to generate *Df(16)7*. For the definitions of the abbreviations, see the legend in Figure 3A. H, *HpaI*; K, *KpnI*; X, *XbaI*. (B) Genomic locations of BAC probes for FISH analysis. (C) FISH analysis of metaphase chromosomes prepared from *Df(16)7/+* ES cells. (D) Southern blot analysis, using Probe 7C, of *HpaI*-digested tail DNA from a *Df(16)7/+* mouse. (E) *Dp(16)1/Df(16)7* ($n = 14$), *Dp(16)1/+* ($n = 14$) and $+/+$ ($n = 14$) mice were examined in the T-maze. (F) The three groups of mice in (E) were examined in a contextual fear-conditioning test. The percentages of time frozen before the foot shock and during the 24 h contextual tests are shown. (G) Analysis of hippocampal LTP. Brain slices from *Dp(16)1/Df(16)7* ($n = 8$), *Dp(16)1/+* ($n = 9$) and $+/+$ ($n = 9$) mice were analyzed using electrophysiological recordings in the CA1 region of the hippocampus. Recordings of fEPSPs were carried out before and after TBS inductions. Evoked potentials were normalized to the fEPSPs recorded prior to TBS induction. * $P < 0.05$ and ** $P < 0.01$.

hippocampal LTPs, we found that the magnitude of LTP after TBS of the brain slices from *Dp(16)1/Dyrk1a^{m1}* mice was higher than that from *Dp(16)1/+* mice ($P < 0.01$), but it was not as high as that

from the wild-type controls ($P < 0.01$; Fig. 5E). These data indicate that *Dyrk1a* is indeed a causative gene for the cognitive deficits observed in *Dp(16)1/+* mice. To examine the simultaneous impact

of *Dyrk1a* and *Kcnj6* on cognitively relevant phenotypes, we compared *Dp(16)1/Df(16)7*, *Dp(16)1/+* and wild-type control mice in the T-maze and contextual fear-conditioning tests. Our results showed that *Dp(16)1/Df(16)7* mice performed significantly worse than wild-type controls in the T-maze and contextual fear-conditioning tests ($P < 0.05$). In addition, *Dp(16)1/Df(16)7* mice did not show improvement over *Dp(16)1/+* mice in these tests ($P > 0.05$; Fig. 6E and F). We compared hippocampal LTPs of these mice and found that the magnitude of LTP after TBS of the brain slices from *Dp(16)1/Df(16)7* mice was significantly lower than that from wild-type control mice ($P < 0.01$, Fig. 6G). Further comparison showed that the magnitude of LTP from *Dp(16)1/Df(16)7* mice appeared slightly higher than that from *Dp(16)1/+* mice, but the difference is not statistically significant ($P > 0.05$; Fig. 6G).

The aforementioned genetic analysis based on *Dp(16)1; Ms1Rhr*, *Dp(16)1/Df(16)5*, *Dp(16)1/Df(16)6*, *Dp(16)1/Dyrk1a^{mt1}* and *Dp(16)1/Df(16)7* mice indicates that both *Dyrk1a* and *Kcnj6* are key genes in DS-associated cognitively relevant phenotypes, with *Dyrk1a* playing a causative role and *Kcnj6* playing a critical mediating role in these phenotypes. *Dp(16)1; Ms1Rhr* mice, but not *Dp(16)1/Df(16)5* mice, showed improved cognitive function when compared with *Dp(16)1/+* mice, suggesting that the *Kcnj15-Mx2* interval contains a causative gene(s) for DS-associated developmental cognitive deficits (Fig. 1).

Discussion

Many surprises have occurred in the history of genetic analysis of DS. This is because DS is caused by the triplication of the entire human chromosome 21. Actions and interactions of approximately 175 gene orthologs associated with Hsa21 often led to unexpected results in relationship to DS phenotypes.

In this study, we focussed on genetic analysis of the *Setd4/Cbr1-Fam3b/Mx2* region, which is built upon the previous results from other laboratories as well as from our own laboratories. Using the subtractive strategy, we confirmed the importance of the *Cbr1-Fam3b* region in causing developmental cognitive deficits in DS using *Dp(16)1; Ms1Rhr* mice. In the attempt to identify the location(s) of the causative gene(s), we generated and analyzed two compound mutants, *Dp(16)1/Df(16)5* and *Dp(16)1/Df(16)6*, each of which carries a deletion spanning approximately half of the *Setd4-Mx2* region (Fig. 1 and Supplementary Material, Table S1). The first major surprise is that neither compound mutant showed improvement over *Dp(16)1/+* mice in T-maze and contextual fear-conditioning tests. Based on this result, we speculate the possible presence of at least two dosage-sensitive causative genes, with at least one in each deletion region. Our speculation is that when the causative gene(s) in the *Setd4-Kcnj6* region is normalized in *Dp(16)1/Df(16)5* mice, the causative gene(s) in the *Kcnj15-Mx2* region could still exert its effect on causing cognitive deficits. Similarly, when the causative gene(s) in the *Kcnj15-Mx2* region is normalized in *Dp(16)1/Df(16)6* mice, the causative gene(s) in the *Setd4-Kcnj6* region could still be able to have an impact on cognitive function.

Because *Dyrk1a* and *Kcnj6* have been proposed as the major causative genes for cognitive deficits in DS, we generated and analyzed *Dp(16)1/Dyrk1a^{mt1}* and *Dp(16)1/Df(16)7* mice. The improved performance of *Dp(16)1/Dyrk1a^{mt1}* mice in T-maze and contextual fear-conditioning tests over *Dp(16)1/+* mice confirms the causative role of *Dyrk1a* (Figs 1 and 5). This result is similar to the data generated using *Ts65Dn* mice-based subtractive approach (26), even though there are significant genomic differences between *Ts65Dn* and *Dp(16)1/+* mice, such as the extra 15 Hsa21 gene orthologs triplicated in *Dp(16)1/+* mice over *Ts65Dn* mice, and the triplication of the *Mmu17* centromeric region

which is orthologous to a region of Hsa6 in *Ts65Dn* mice but not in *Dp(16)1/+* mice. The analysis of the next compound mutant led to the second major surprise of our study that *Dp(16)1/Df(16)7* mice showed no significant improvement of cognitively relevant phenotypes over *Dp(16)1/+* mice when both *Dyrk1a* and *Kcnj6* were converted to two copies in the *Dp(16)1/Df(16)7* mice.

Through this study, we established two important facts. First, *Dyrk1a* is a causative gene because partial rescue occurs when *Dyrk1a* was converted to two copies in *Dp(16)1/Dyrk1a^{mt1}* mice. Secondly, *Kcnj6* plays an important role because no rescue occurs when both *Dyrk1a* and *Kcnj6* were converted to two copies in *Dp(16)1/Df(16)7* mice. To interpret all our data generated in this study, we hypothesize the presence of a causative gene 'X' for DS-associated cognitive deficits in the *Kcnj15-Mx2* region and further hypothesize that the effect of the triplication of this gene is suppressed by the triplication of *Kcnj6*. In *Dp(16)1/+* mice, the presence of three copies of *Dyrk1a* contributes to cognitive deficits, whereas the effect of the triplication of X is suppressed by the triplication of *Kcnj6* (Fig. 7A). In *Dp(16)1; Ms1Rhr* mice, converting *Dyrk1a* to two copies causes partial rescue of cognitive deficits. Because there is another causative gene(s) outside of the *Cbr1-Fam3b* region in the Hsa21 orthologous region on *Mmu16*, the rescue is only partial. X is present only in two copies in *Dp(16)1; Ms1Rhr* mice, so it does not contribute to cognitive deficits (Fig. 7B). In *Dp(16)1/Df(16)5* mice, *Dyrk1a* is present in two copies and does not contribute to cognitive deficits, whereas X is present in three copies and *Kcnj6* is present in two copies, so the effect of the triplication of X is not suppressed by *Kcnj6*. Therefore, X contributes to cognitive deficits in *Dp(16)1/Df(16)5* mice (Fig. 7C). In *Dp(16)1/Df(16)6* mice, *Dyrk1a* is present in three copies and contributes to cognitive deficits, whereas X is present only in two copies and does not contribute to cognitive deficits (Fig. 7D). In *Dp(16)1/Dyrk1a^{mt1}* mice, converting *Dyrk1a* to two copies causes partial rescue of cognitive deficits, while the effect of the triplication of X is suppressed by the triplication of *Kcnj6* (Fig. 7E). In *Dp(16)1/Df(16)7* mice, *Dyrk1a* is present in two copies and does not contribute to cognitive deficits, whereas X is present in three copies and *Kcnj6* is present in two copies, so the effect of the triplication of X is not suppressed by *Kcnj6*. Therefore, X contributes to cognitive deficits in *Dp(16)1/Df(16)7* mice (Fig. 7F).

Our results set up a framework by which *Kcnj6* may contribute to cognitive deficits associated with the triplication of the *Setd4/Cbr1-Fam3b/Mx2* region (Fig. 7). This information may also explain why ethosuximide, an inhibitor of the *Kcnj6*-encoded protein, cannot rescue cognitive deficits of *Ts65Dn* mice (27), because *Dyrk1a* is present in three copies in *Ts65Dn* mice and also reducing the effectiveness of *Kcnj6* could enhance the effect of the triplication of another causative gene, i.e. X in the *Kcnj15-Mx2* region (Fig. 7).

One of the next challenges is to establish the identity of the X gene, which is necessary to understand the mechanism of *Kcnj6*-associated suppression. Among 16 Hsa21 gene orthologs in the *Kcnj15-Mx2* region, *Ets2*, *Psmg1*, *Brudd1*, *Hmgn1*, *Wrh*, *Pcp4* and *Dscam* are the potential candidates because they are well expressed in the brain (28–38). One of the approaches to identify the X gene is to compound a null allele of a candidate gene with *Dp(16)1* and *Df(16)7* simultaneously. This can be achieved by transferring *Df(16)7* or the null allele of the gene to the chromosome homolog carrying *Dp(16)1* by crossover. The identity of the X gene will be revealed by partial rescue of cognitive deficits in such a triple compound mutant. Alternative to individual null alleles, smaller engineered deletions within the *Kcnj15-Mx2* region could be used in the same compounding strategy to systemically dissect the region with the goal to identify the X gene.

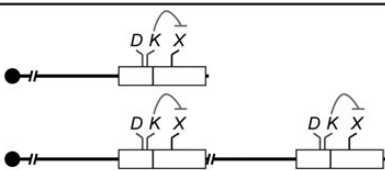
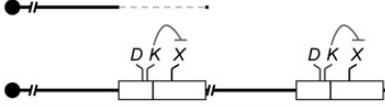
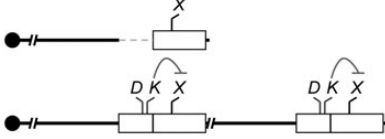
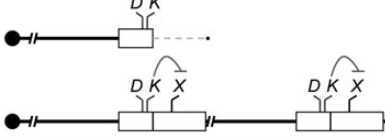
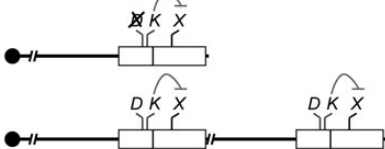
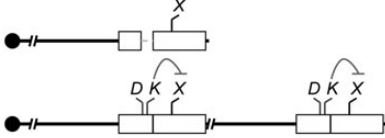
	Mouse Mutants	Copy #			Cognitive deficits
		D	K	X	
A	<i>Dp(16)1/+</i> 	3	3	3	Yes
		3	3	3	
B	<i>Dp(16)1;Ms1Rhr</i> 	2	2	2	PR
		2	2	2	
C	<i>Dp(16)1/Df(16)5</i> 	2	2	3	NR
		2	2	3	
D	<i>Dp(16)1/Df(16)6</i> 	3	3	2	NR
		3	3	2	
E	<i>Dp(16)1/Dyrk1a^{m1}</i> 	2	3	3	PR
		2	3	3	
F	<i>Dp(16)1/Df(16)7</i> 	2	2	3	NR
		2	2	3	

Figure 7. Actions and interactions of the genes in the *Setd4/Cbr1-Fam3b/Mx2* region in relationship to DS-associated cognitive deficits. D, *Dyrk1a*; K, *Kcnj6*; X, a gene located in the deletion interval of *Df(16)6*. PR, partial rescue observed; NR, no rescue observed.

Our aforementioned reasoning and gene-hunting strategy are built upon the hypothetic presence of a single causative gene in the *Kcnj15-Mx2* region, but an additional unknown causative gene(s) may exist in the *Kcnj15-Mx2* region and/or the *Setd4-Kcnj6* region. Thus, the gene-hunting strategy may need to be expanded to identify the potential additional causative gene(s).

By generating and analyzing multiple compound mutants, we showed here a highly complex picture of gene actions and interactions associated with the *Setd4/Cbr1-Fam3b/Mx2* region as well as the impact of these events on developmental cognitive deficits in DS. Such complexities present a challenge to fully elucidate the precise mechanisms underlying DS-associated developmental cognitive deficits.

Materials and Methods

Generation of mouse mutants

We generated new chromosomal deletions using Cre/*loxP*-mediated chromosome engineering (39). Specific MICER clones (17) were selected for use as the targeting vectors to deliver *loxP* to the two endpoints of each deletion in the genome of mouse ES cells, i.e. AB2.2 ES cells (40). Prior to gene targeting, MICER clones were linearized in the

mouse genomic DNA inserts with specific restriction enzymes (Supplementary Material, Table S2). The linearized targeting vectors were electroporated into ES cells, which were then selected with G418 or puromycin. Double-targeted ES cell clones were identified by Southern blot analysis using PCR products as probes. ES cell culture and electroporation were carried out as described (41). To induce recombination between targeted *loxP* sites, a Cre-expression vector, pOG231 (42), was electroporated into double-targeted cells. ES cell clones carrying individual deletions were identified by Southern blot analysis with ES cell DNA digested with specific restriction enzymes and hybridized with specific probes (Supplementary Material, Table S2) and confirmed by FISH analysis.

To generate a *Dyrk1a* mutant allele in mice, the SIGTR ES cell line XQ0369, which carries *Dyrk1aGt(XQ0369)Wtsi* (i.e. *Dyrk1a^{m1}*), was obtained from the Mutant Mouse Regional Resource Centers, (<http://www.informatics.jax.org/allele/MGI:4338238>). This mutant ES cell line was generated by the Wellcome Trust Sanger Institute via a gene trap event in intron 4 of *Dyrk1a* using the gene trap vector pGT01xf (<http://www.sanger.ac.uk/resources/mouse/sigtr/>). We examined this mutant ES cell line by carrying out RT-PCR analysis of ES cell RNA with PCR primers based on exon 4 of *Dyrk1a* (forward primer: 5'-GGGCCAGGGGACGATTCCAGT-3') and the *beta-Geo* cassette in the gene trap vector (reverse

primer: 5'-CGCCAGGGTTTCCAGTCACGA-3') (Fig. 5A). The RT-PCR product was sequenced to confirm the presence of the specific fusion mRNA as the consequence of the gene trap event (Fig. 5B and Supplementary Material, Fig. S1). Our sequence is identical to the junction sequence generated by the Wellcome Trust Sanger Institute for this cell line (<http://www.genetrapp.org/cgi-bin/annotation.py?cellline=XQ0369>).

The ES cell lines carrying the aforementioned individual mutations were used to generate germline chimeras by injecting them into blastocysts isolated from C57BL/6J mice, as described previously (19,41,43). Deletion mutant mice were identified by Southern blot analysis of mouse tail DNA (Supplementary Material, Table S2). *Dyrk1a*^{m1/+} mice were identified using *beta*-Geo-specific PCR-based analysis of mouse tail DNA with the following primer pair: 5'-ACGAGTCTCTGAGCGGGACTCT-3' and 5'-GATAACCGTATTACCGCTTTG-3' (Fig. 5A) and confirmed by sequencing the junction between exon 4 of *Dyrk1a* and the gene trap vector pGT01xf using cDNA generated from brain mRNA of *Dyrk1a*^{m1/+} mice (Fig. 5B).

Fluorescent in situ hybridization

FISH analysis was performed as described previously (18,19). The metaphase chromosome spreads of ES cells were prepared, as described previously (18,19). To detect the chromosomal deletions between *Setd4* and *Kcnj6*, between *Kcnj15* and *Mx2* or between *Dyrk1a* and *Kcnj6* on Mmu16, individual BAC clones carrying mouse genomic DNA mapped within these regions were selected and labeled with digoxigenin and detected with anti-digoxigenin-rhodamine antibody (Supplementary Material, Table S2). A BAC clone carrying mouse genomic DNA mapped to a Hsa21 orthologous region on Mmu16 but proximal to the *Setd4/Cbr1-Fam3b/Mx2* region was used to identify Mmu16 and labeled with biotin and detected with fluorescein isothiocyanate-avidin (Supplementary Material, Table S2). Chromosomes were counterstained with 4',6'-diamidino-2-phenylindole.

Animals

Dp(16)1/+ mice were identified by Southern blot analysis (13) as well as by a PCR-based genotyping strategy. The latter was designed on the basis of the unique 355 bp junction sequence between the 5'-HPRT vector backbone and the mouse genomic DNA insert in the targeting vector pTVZfp295 (13) using the forward primer 5'-CTGCCAGCCACTCTAGCTCT-3' and the reverse primer 5'-AATTTCTGTGGGGCAAATG-3'. Mutant mice carrying *Dp(16)1*, *Df(16)5*, *Df(16)6* and *Df(16)7* were first established in a (129Sv × C57BL/6J)F1 background and backcrossed to C57BL/6J mice for five generations. *Dyrk1a*^{m1/+} mice were first established by crossing chimeras with C57BL/6J mice, and the mutant progeny were maintained by crossing to (129Sv × C57BL/6J)F1 mice. *Ms1Rhr* mice were purchased from the Jackson Laboratory (Bar Harbor, ME, USA) and maintained by crossing to (C57BL/6J)EiJ × C3Sn.BLiA-Pde6b⁺)F1 mice (44). *Dp(16)1;Ms1Rhr* mice were generated by crossing *Dp(16)1/+* mice to *Ms1Rhr* mice.

All mice were maintained at a temperature- and humidity-controlled animal facility with a 12 h light and dark schedule and had *ad libitum* access to food and water. All mice used in the experiments were 2–4 months old. Before behavioral experiments, each mouse was pre-handled for 2 min every day for 1 week. All the experimental procedures were approved by the Institutional Animal Care and Use Committee at Roswell Park Cancer Institute.

RT-PCR and real-time quantitative RT-PCR

RT-PCR and real-time quantitative RT-PCR were used to analyze expression of the selected genes in ES cells and mice carrying different genotypes. *Gapdh*, located on Mmu6, was used as the internal disomic control for all of the mice examined. Total RNAs, isolated from ES cells or mouse brains using TRIzol Reagent (Life Technologies, Grand Island, NY, USA), were used to generate cDNA by Superscript version III reverse transcriptase (Life Technologies), which were then used as the templates for PCR experiments. For real-time quantitative RT-PCR analysis, the cDNA samples from three mice with each genotype were analyzed using the gene-specific primers and probes from TaqMan Gene Expression Assays System (Life Technologies). The PCR reactions were carried out in the StepOnePlus™ Real-Time PCR systems (Life Technologies) with the following amplification conditions: an initial activation and denaturation at 95°C for 10 min, followed by 40 cycles of denaturation at 95°C for 15 s, primer annealing and extension at 60°C for 1 min.

T-maze spontaneous alternation test

A modified protocol of Deacon and Rawlins (45) was used for the continuous spontaneous alternation task to examine hippocampal function. The maze was made of opaque acrylic (Plexiglas) with a sliding door separating the start arm (90 cm × 10 cm × 20 cm) from the rest of the apparatus, which comprised a choice point at the intersection of the start arm with the left and right arms of the maze (37 cm × 10 cm × 20 cm for each arm). A divider panel (20 cm × 20 cm) was centered at the intersection of the 'T' so that it extended 10 cm into the start arm. At the start of the test, a mouse was confined to the start arm for 5 min and then permitted free access to the rest of the maze for 10 min. The T-maze was cleaned with 10% ethanol between mice. A choice was recorded when the whole body of the mouse including its tail left the start arm and entered into one of the lateral arms. Entry into a lateral arm opposite to the one previously chosen was defined as an alternation. Alternation performance was defined as the percentage of times the mouse alternated between the lateral arms over the total number of possible alternations.

Contextual fear-conditioning test

The contextual fear-conditioning test was performed as described previously (9). In brief, each mouse was given 2 min to explore the test chamber (baseline activity). The floor was a grid of stainless steel rods connected to an electric shock generator. A video camera was mounted in the front of the chamber and a ceiling light illuminated the interior through the transparent ceiling. Delivery of a foot shock (1 mA scrambled) for 2 s was controlled by Video Freeze Software (Med Associates, St. Albans, VT, USA). The mouse was allowed to stay in the chamber for an additional 30 s and then removed. Approximately 24 h later, each mouse was returned to the chamber and monitored for freezing behavior for 3 min, without any foot shock being delivered. Freezing behavior was recorded automatically by Video Freeze Software. Mean freezing activity during the contextual exposure was calculated as a measure of contextual learning.

Foot-shock sensitivity test

To facilitate accurate interpretation of the data from the fear-conditioning tests, we performed a foot-shock sensitivity test using the fear-conditioning test chamber. A foot shock was delivered every 10 s starting at 0.05 mA, with a 0.05 mA increment

between each shock. The minimal level of current needed to elicit flinching or vocalizing was recorded.

Hippocampal slice preparation

The procedure for hippocampal slice preparation used in electrophysiological recordings was as described previously (12). Briefly, after being removed from the skulls, brains were placed in an ice-cold solution (pH 7.4) consisting of the following (in mM): sucrose 110, NaCl 60, KCl 3, NaH₂PO₄ 1.25, NaHCO₃ 28, MgSO₄ 7, (+)-sodium-L-ascorbate 0.6, CaCl₂ 0.5 and glucose 5. The solution was continuously bubbled with oxygen gas (95% O₂-5% CO₂). The hippocampal formation was resected and sectioned into 350 μm transverse slices using a vibratome. After the slices were transferred to an interface-recording chamber (Automate Scientific, Inc., Berkeley, CA, USA), they were submerged in artificial cerebrospinal fluid, which comprised the following (in mM): NaCl 119, KCl 3, NaHCO₃ 26.2, MgSO₄ 1.3, NaH₂PO₄ 1, CaCl₂ 2.5 and glucose 11. Incubation was carried out for at least 1 h at a constant temperature of 28 ± 1°C. The top surfaces of the slices were exposed to humidified oxygen gas (95% O₂-5% CO₂).

Electrophysiological recordings and induction of synaptic plasticity

Standard extracellular recording techniques were employed as described previously (12). In short, Schaffer collateral-commissural fibers were stimulated with a bipolar Teflon-coated tungsten electrode (Microprobes, Gaithersburg, MD, USA). fEPSPs were recorded using a glass microelectrode filled with 2 M NaCl positioned in the stratum radiatum of the CA1 hippocampal area. LTP was induced by TBS which includes 15 bursts of four pulses at 100 Hz and delivered at an interburst interval of 200 ms through the stimulating electrode. We performed electrophysiological recordings for 80 min on each brain slice, including 20 min of baseline recording and 60 min after the TBS induction. Signals from recording electrodes were amplified with Model 1800 microelectrode AC amplifier (A-M Systems, Carlsborg, WA, USA) and digitized at a 10 kHz sampling rate by an Axon Digidata 1400 A Data Acquisition System (Molecular Devices, Sunnyvale, CA, USA). Traces were obtained by pClamp 10.2 and analyzed using Clampfit 10.2 software (Molecular Devices).

Statistical analysis

Data from the T-maze spontaneous alternation test, contextual fear-conditioning test, foot-shock sensitivity test and hippocampal LTP from electrophysiological experiments were subjected to one-way analysis of variance between genotypes. In the behavioral phenotyping experiments, *n* indicates the number of mice. In the electrophysiological analysis, *n* indicates the number of slices analyzed. All values reported in the figures and tables are expressed as means ± SEM.

Supplementary Material

Supplementary Material is available at HMG online.

Acknowledgement

The authors would like to thank Zhongyou Li for his assistance.

Conflict of Interest statement. None of the authors has any conflict of interest.

Funding

This study was supported in part by grants from the National Institutes of Health (R01NS66072, R01HL91519, R21GM114645 and P30CA16056), Roswell Park Alliance Foundation, Louis Sklarow Memorial Fund, Jerome Lejeune Foundation, the Children's Guild Foundation and the National Natural Science Foundation of China (81100844).

References

- Antonarakis, S.E., Lyle, R., Dermitzakis, E.T., Reymond, A. and Deutsch, S. (2004) Chromosome 21 and down syndrome: from genomics to pathophysiology. *Nat. Rev. Genet.*, **5**, 725–738.
- Roizen, N.J. and Patterson, D. (2003) Down's syndrome. *Lancet*, **361**, 1281–1289.
- Parker, S.E., Mai, C.T., Canfield, M.A., Rickard, R., Wang, Y., Meyer, R.E., Anderson, P., Mason, C.A., Collins, J.S., Kirby, R.S. et al. (2010) Updated National Birth Prevalence estimates for selected birth defects in the United States, 2004–2006. *Birth Defects Res. A Clin. Mol. Teratol.*, **88**, 1008–1016.
- Khoshnood, B., Greenlees, R., Loane, M., Dolk, H., Committee, E.P.M. and Group, E.W. (2011) Paper 2: EUROCAT public health indicators for congenital anomalies in Europe. *Birth Defects Res. A Clin. Mol. Teratol.*, **91**(Suppl. 1), S16–S22.
- Natoli, J.L., Ackerman, D.L., McDermott, S. and Edwards, J.G. (2012) Prenatal diagnosis of Down syndrome: a systematic review of termination rates (1995–2011). *Prenat. Diagn.*, **32**, 142–153.
- Korenberg, J.R., Chen, X.N., Schipper, R., Sun, Z., Gonsky, R., Gerwehr, S., Carpenter, N., Daumer, C., Dignan, P. and Disteche, C. (1994) Down syndrome phenotypes: the consequences of chromosomal imbalance. *Proc. Natl Acad. Sci. USA*, **91**, 4997–5001.
- Sinet, P.M., Theophile, D., Rahmani, Z., Chettouh, Z., Blouin, J.L., Prieur, M., Noel, B. and Delabar, J.M. (1994) Mapping of the Down syndrome phenotype on chromosome 21 at the molecular level. *Biomed. Pharmacother.*, **48**, 247–252.
- Noble, J. (1998) Natural history of Down's syndrome: a brief review for those involved in antenatal screening. *J. Med. Screen.*, **5**, 172–177.
- Yu, T., Liu, C., Belichenko, P., Clapcote, S.J., Li, S., Pao, A., Kleschevnikov, A., Bechard, A.R., Asrar, S., Chen, R. et al. (2010) Effects of individual segmental trisomies of human chromosome 21 syntenic regions on hippocampal long-term potentiation and cognitive behaviors in mice. *Brain Res.*, **1366**, 162–171.
- Belichenko, N.P., Belichenko, P.V., Kleschevnikov, A.M., Salehi, A., Reeves, R.H. and Mobley, W.C. (2009) The 'Down syndrome critical region' is sufficient in the mouse model to confer behavioral, neurophysiological, and synaptic phenotypes characteristic of Down syndrome. *J. Neurosci.*, **29**, 5938–5948.
- Olson, L.E., Roper, R.J., Sengstaken, C.L., Peterson, E.A., Aquino, V., Galdzicki, Z., Siarey, R., Pletnikov, M., Moran, T.H. and Reeves, R.H. (2007) Trisomy for the Down syndrome 'critical region' is necessary but not sufficient for brain phenotypes of trisomic mice. *Hum. Mol. Genet.*, **16**, 774–782.
- Zhang, L., Meng, K., Jiang, X., Liu, C., Pao, A., Belichenko, P.V., Kleschevnikov, A.M., Josselyn, S., Liang, P., Ye, P. et al. (2014) Human chromosome 21 orthologous region on mouse chromosome 17 is a major determinant of Down syndrome-related developmental cognitive deficits. *Hum. Mol. Genet.*, **23**, 578–589.

13. Li, Z., Yu, T., Morishima, M., Pao, A., LaDuca, J., Conroy, J., Nowak, N., Matsui, S., Shiraiishi, I. and Yu, Y. (2007) Duplication of the entire 22.9-Mb human chromosome 21 syntenic region on mouse chromosome 16 causes cardiovascular and gastrointestinal abnormalities. *Hum. Mol. Genet.*, **16**, 1359–1366.
14. Bliss, T.V. and Collingridge, G.L. (1993) A synaptic model of memory: long-term potentiation in the hippocampus. *Nature*, **361**, 31–39.
15. Malenka, R.C. and Nicoll, R.A. (1999) Long-term potentiation—a decade of progress? *Science*, **285**, 1870–1874.
16. Costa, A.C., Stasko, M.R., Schmidt, C. and Davisson, M.T. (2010) Behavioral validation of the Ts65Dn mouse model for Down syndrome of a genetic background free of the retinal degeneration mutation *Pde6b(rd1)*. *Behav. Brain Res.*, **206**, 52–62.
17. Adams, D.J., Biggs, P.J., Cox, T., Davies, R., van der Weyden, L., Jonkers, J., Smith, J., Plumb, B., Taylor, R., Nishijima, I. et al. (2004) Mutagenic insertion and chromosome engineering resource (MICER). *Nat. Genet.*, **36**, 867–871.
18. Robertson, E. (1987) In Robertson, E. (ed.), *Teratocarcinomas and Embryonic Stem Cells—A Practical Approach*. IRL Press, Oxford, pp. 71–112.
19. Yu, Y.E., Morishima, M., Pao, A., Wang, D.Y., Wen, X.Y., Baldini, A. and Bradley, A. (2006) A deficiency in the region homologous to human 17q21.33–q23.2 causes heart defects in mice. *Genetics*, **173**, 297–307.
20. Fernandez-Martinez, J., Vela, E.M., Tora-Ponsioen, M., Ocana, O.H., Nieto, M.A. and Galceran, J. (2009) Attenuation of Notch signalling by the Down-syndrome-associated kinase DYRK1A. *J. Cell Sci.*, **122**, 1574–1583.
21. Hammerle, B., Ulin, E., Guimera, J., Becker, W., Guillemot, F. and Tejedor, F.J. (2011) Transient expression of *Mnb/Dyrk1a* couples cell cycle exit and differentiation of neuronal precursors by inducing p27KIP1 expression and suppressing NOTCH signaling. *Development*, **138**, 2543–2554.
22. Kelly, P.A. and Rahmani, Z. (2005) DYRK1A enhances the mitogen-activated protein kinase cascade in PC12 cells by forming a complex with Ras, B-Raf, and MEK1. *Mol. Biol. Cell*, **16**, 3562–3573.
23. Mark, M.D. and Herlitze, S. (2000) G-protein mediated gating of inward-rectifier K⁺ channels. *Eur. J. Biochem.*, **267**, 5830–5836.
24. Yamada, M., Inanobe, A. and Kurachi, Y. (1998) G protein regulation of potassium ion channels. *Pharmacol. Rev.*, **50**, 723–760.
25. Fotaki, V., Dierssen, M., Alcantara, S., Martinez, S., Marti, E., Casas, C., Visa, J., Soriano, E., Estivill, X. and Arbones, M.L. (2002) *Dyrk1A* haploinsufficiency affects viability and causes developmental delay and abnormal brain morphology in mice. *Mol. Cell Biol.*, **22**, 6636–6647.
26. Garcia-Cerro, S., Martinez, P., Vidal, V., Corrales, A., Florez, J., Vidal, R., Rueda, N., Arbones, M.L. and Martinez-Cue, C. (2014) Overexpression of *Dyrk1A* is implicated in several cognitive, electrophysiological and neuromorphological alterations found in a mouse model of Down syndrome. *PLoS ONE*, **9**, e106572.
27. Vidal, V., Garcia, S., Martinez, P., Corrales, A., Florez, J., Rueda, N., Sharma, A. and Martinez-Cue, C. (2012) Lack of behavioral and cognitive effects of chronic ethosuximide and gabapentin treatment in the Ts65Dn mouse model of Down syndrome. *Neuroscience*, **220**, 158–168.
28. Kahlem, P., Sultan, M., Herwig, R., Steinfath, M., Balzereit, D., Eppens, B., Saran, N.G., Pletcher, M.T., South, S.T., Stetten, G. et al. (2004) Transcript level alterations reflect gene dosage effects across multiple tissues in a mouse model of Down syndrome. *Genome Res.*, **14**, 1258–1267.
29. Lyle, R., Gehrig, C., Neergaard-Henrichsen, C., Deutsch, S. and Antonarakis, S.E. (2004) Gene expression from the aneuploid chromosome in a trisomy mouse model of Down syndrome. *Genome Res.*, **14**, 1268–1274.
30. Barlow, G.M., Micales, B., Lyons, G.E. and Korenberg, J.R. (2001) Down syndrome cell adhesion molecule is conserved in mouse and highly expressed in the adult mouse brain. *Cytogenet. Cell Genet.*, **94**, 155–162.
31. Yamakawa, K., Huot, Y.K., Haendelt, M.A., Hubert, R., Chen, X.N., Lyons, G.E. and Korenberg, J.R. (1998) DSCAM: a novel member of the immunoglobulin superfamily maps in a Down syndrome region and is involved in the development of the nervous system. *Hum. Mol. Genet.*, **7**, 227–237.
32. Wolvetang, E.J., Wilson, T.J., Sanij, E., Busciglio, J., Hatzistavrou, T., Seth, A., Hertzog, P.J. and Kola, I. (2003) ETS2 overexpression in transgenic models and in Down syndrome predisposes to apoptosis via the p53 pathway. *Hum. Mol. Genet.*, **12**, 247–255.
33. Abuhatzira, L., Shamir, A., Schones, D.E., Schaffer, A.A. and Bustin, M. (2011) The chromatin-binding protein HMG1 regulates the expression of methyl CpG-binding protein 2 (MECP2) and affects the behavior of mice. *J. Biol. Chem.*, **286**, 42051–42062.
34. Egeo, A., Mazzocco, M., Sotgia, F., Arrigo, P., Oliva, R., Bergonon, S., Nizetic, D., Rasore-Quartino, A. and Scartezzini, P. (1998) Identification and characterization of a new human cDNA from chromosome 21q22.3 encoding a basic nuclear protein. *Hum. Genet.*, **102**, 289–293.
35. Ling, K.H., Hewitt, C.A., Tan, K.L., Cheah, P.S., Vidyadaran, S., Lai, M.I., Lee, H.C., Simpson, K., Hyde, L., Pritchard, M.A. et al. (2014) Functional transcriptome analysis of the postnatal brain of the Ts1Cje mouse model for Down syndrome reveals global disruption of interferon-related molecular networks. *BMC Genomics*, **15**, 624.
36. Renelt, M., von Bohlen und Halbach, V. and von Bohlen und Halbach, O. (2014) Distribution of PCP4 protein in the forebrain of adult mice. *Acta Histochem.*, **116**, 1056–1061.
37. Song, H.J., Park, J., Seo, S.R., Kim, J., Paik, S.R. and Chung, K.C. (2008) Down syndrome critical region 2 protein inhibits the transcriptional activity of peroxisome proliferator-activated receptor beta in HEK293 cells. *Biochem. Biophys. Res. Commun.*, **376**, 478–482.
38. Vidal-Taboada, J.M., Lu, A., Pique, M., Pons, G., Gil, J. and Oliva, R. (2000) Down syndrome critical region gene 2: expression during mouse development and in human cell lines indicates a function related to cell proliferation. *Biochem. Biophys. Res. Commun.*, **272**, 156–163.
39. Yu, Y. and Bradley, A. (2001) Engineering chromosomal rearrangements in mice. *Nat. Rev. Genet.*, **2**, 780–790.
40. Bradley, A., Zheng, B. and Liu, P. (1998) Thirteen years of manipulating the mouse genome: a personal history. *Int. J. Dev. Biol.*, **42**, 943–950.
41. Ramirez-Solis, R., Davis, A.C. and Bradley, A. (1993) Gene targeting in embryonic stem cells. *Methods Enzymol.*, **225**, 855–878.
42. O’Gorman, S., Dagenais, N.A., Qian, M. and Marchuk, Y. (1997) Protamine-Cre recombinase transgenes efficiently recombine target sequences in the male germ line of mice, but not in embryonic stem cells. *Proc. Natl Acad. Sci. USA*, **94**, 14602–14607.
43. Bradley, A. (1987) In Robertson, E. (ed.), *Teratocarcinomas and Embryonic Stem Cells—A Practical Approach*. IRL Press, Oxford, pp. 113–151.
44. Olson, L.E., Richtsmeier, J.T., Leszl, J. and Reeves, R.H. (2004) A chromosome 21 critical region does not cause specific Down syndrome phenotypes. *Science*, **306**, 687–690.
45. Deacon, R.M. and Rawlins, J.N. (2006) T-maze alternation in the rodent. *Nat. Protoc.*, **1**, 7–12.